

Optimal Transport Kernels for Sequential and Parallel Neural Architecture Search

Vu Nguyen*
University of Oxford

Tam Le*
RIKEN AIP

Makoto Yamada
Kyoto Uni. & RIKEN AIP

Michael A. Osborne
University of Oxford

Abstract

Neural architecture search (NAS) automates the design of deep neural networks. One of the main challenges in searching complex and non-continuous architectures is to compare the similarity of networks that the conventional Euclidean metric may fail to capture. Optimal transport (OT) is resilient to such complex structure by considering the minimal cost for transporting a network into another. However, the OT is generally not negative definite which may limit its ability to build the positive-definite kernels required in many kernel-dependent frameworks. Building upon tree-Wasserstein (TW), which is a negative definite variant of OT, we develop a novel discrepancy for neural architectures, and demonstrate it within a Gaussian process (GP) surrogate model for the sequential NAS settings. Furthermore, we derive a novel parallel NAS, using quality k-determinantal point process on the GP posterior, to select diverse and high-performing architectures from a discrete set of candidates. We empirically demonstrate that our TW-based approaches outperform other baselines in both sequential and parallel NAS.

1 Introduction

Neural architecture search (NAS) is the process of automating architecture engineering to find the best design of our neural network model. This output architecture will perform well for a given dataset. With the increasing interest in deep learning in recent years, NAS has attracted significant research attention

[10, 12, 32, 33, 34, 44, 45, 49, 56, 63, 65]. We refer the interested readers to the survey [13] for a detailed review of NAS and to the comprehensive list¹ for all of the related papers in NAS.

Bayesian optimization (BO) utilizes a probabilistic model, particularly Gaussian process (GP) [43], for determining future evaluations and its evaluation efficiency makes it well suited for the expensive evaluations of NAS. However, the conventional BO approaches [50, 52] are not suitable to capture the complex and non-continuous designs of neural architectures. Recent work [25] has considered optimal transport (OT) for measuring neural architectures. This views two networks as logistical *suppliers* and *receivers*, then optimizes to find the minimal transportation cost as the distance, i.e., similar architectures will need less cost for transporting and vice versa. However, the existing OT distance for architectures, such as OTMANN [25], do not easily lend themselves to the creation of the positive semi-definite (p.s.d.) kernel (covariance function) due to the indefinite property of OT [39] (§8.3). It is critical as the GP is not a valid random process when the covariance function (kernel) is not p.s.d. (see Lem. 2.1). In addition, there is still an open research direction for *parallel NAS* where the goal is to select multiple high-performing and diverse candidates from a *discrete* set of candidates for parallel evaluations. This discrete property makes the parallel NAS interesting and different from the existing batch BO approaches [8, 21], which are typically designed to handle continuous observations.

We propose a p.s.d. tree-Wasserstein distance for neural network architectures. We design a new way to capture both global and local information via *n*-gram and indegree/outdegree representations for networks. In addition, we propose the k-determinantal point process (k-DPP) quality for selecting diverse and high-performing architectures from a *discrete* set. This discrete property of NAS makes k-DPP ideal in sampling the optimal choices that overcomes the greedy

* denotes equal contribution. Preliminary work. Correspondence to vu@robots.ox.ac.uk.

¹<https://www.automl.org/automl/literature-on-neural-architecture-search>

selection used in the existing batch Bayesian optimization [8, 21, 61]. We summarize our contributions as follows:

- A tree-Wasserstein distance with a novel design for capturing local and global information from architectures which results in a p.s.d. kernel while the existing OT distance does not.
- A demonstration of tree-Wasserstein as the novel GP covariance function for sequential NAS.
- A parallel NAS approach using k-DPP for selecting diverse and high-quality architectures from a discrete set.

2 Tree-Wasserstein for Neural Network Architectures

We first argue that the covariance matrices associated with a kernel function of Gaussian process (GP) and k-DPP need to be positive semi-definite (p.s.d.) for a valid random process in Lemma 2.1. We then develop tree-Wasserstein (TW) [9, 14, 30], the negative definite variant of OT, for measuring the similarity of architectures. Consequently, we can build a p.s.d. kernel upon optimal transport (OT) geometry for modelling with GPs and k-determinantal point processes (k-DPPs).

Lemma 2.1. *If a covariance function k of a Gaussian process is not positive semi-definite, the resulting GP is not a valid random process.*

Proof of Lemma 2.1 is placed in the Appendix §D.1.

2.1 Tree-Wasserstein

We give a brief review about OT, tree metric, tree-Wasserstein (TW) which are the main components for our NAS framework. We denote $[n] = \{1, 2, \dots, n\}$, $\forall n \in \mathbb{N}_+$. Let (Ω, d) be a measurable metric space. For any $x \in \Omega$, we use δ_x for the Dirac unit mass on x .

Optimal transport. OT, a.k.a. Wasserstein, Monge-Kantorovich, or Earth’s Mover distance, is a powerful tool to compare probability measures [39, 57]. Let ω, ν be Borel probability distributions on Ω and $\mathcal{R}(\omega, \nu)$ be the set of probability distributions π on $\Omega \times \Omega$ such that $\pi(B \times \Omega) = \omega(B)$ and $\pi(\Omega \times B') = \nu(B')$ for all Borel sets B, B' . The 1-Wasserstein distance W_d [57] (p.2) between ω, ν is defined as:

$$W_d(\omega, \nu) = \inf_{\pi \in \mathcal{R}(\omega, \nu)} \int_{\Omega \times \Omega} d(x, z) \pi(dx, dz) \quad (1)$$

where d is a ground metric (i.e., cost metric) of OT.

Tree metrics and Tree-Wasserstein. A metric $d : \Omega \times \Omega \rightarrow \mathbb{R}_+$ is a *tree metric* if there exists a tree \mathcal{T} with positive edge lengths such that $\forall x \in \Omega$, then x is a node of \mathcal{T} ; and $\forall x, z \in \Omega$, $d(x, z)$ is equal to the length of the (unique) path between x and z [48] (§7, p.145–182).

Let $d_{\mathcal{T}}$ be the tree metric on tree \mathcal{T} rooted at r . For $x, z \in \mathcal{T}$, we denote $\mathcal{P}(x, z)$ as the (unique) path between x and z . We write $\Gamma(x)$ for a set of nodes in the subtree of \mathcal{T} rooted at x , defined as $\Gamma(x) = \{z \in \mathcal{T} \mid x \in \mathcal{P}(r, z)\}$. For edge e in \mathcal{T} , let v_e be the deeper level node of edge e (the farther node to root r), and w_e be the positive length of that edge.

Tree-Wasserstein (TW) is a special case of OT whose ground metric is a tree metric [9, 14, 30]. Given two measures ω, ν supported on tree \mathcal{T} , and setting the tree metric $d_{\mathcal{T}}$ as the ground metric, then the TW distance $W_{d_{\mathcal{T}}}$ between ω, ν has a closed-form solution as [30]:

$$W_{d_{\mathcal{T}}}(\omega, \nu) = \sum_{e \in \mathcal{T}} w_e |\omega(\Gamma(v_e)) - \nu(\Gamma(v_e))|. \quad (2)$$

It is important to note that we can derive p.s.d. kernels on tree-Wasserstein distance $W_{d_{\mathcal{T}}}$ [30], as opposed to the standard OT W_d for general d [39].

2.2 Tree-Wasserstein for Neural Networks

We present a new approach leveraging the tree-Wasserstein for measuring the similarity of neural network architectures. We consider a neural network architecture \mathbf{x} by (\mathcal{S}^o, A) where \mathcal{S}^o is a multi-set of operations in each layer of \mathbf{x} , and A is an adjacency matrix, representing the connection among these layers in \mathbf{x} . We can also view a neural network as a directed labeled graph where each layer is a node in a graph, and an operation in each layer is a node label (i.e., A represents the graph structure, and \mathcal{S}^o contains a set of node labels). We then propose to extract information from neural network architectures by distilling them into three separate quantities as follows:

n -gram representation for layer operations. Each neural network consists of several operations from input layer to output layer. Inspired by the n -gram representation for a document in natural language processing, we view a neural network as a document and its operations as words. Therefore, we can use n -grams (i.e., n -length paths) to represent operations used in the neural network. We then normalize the n -gram, and denote it as \mathbf{x}^o for a neural network \mathbf{x} .

Particularly, for $n = 1$, the n -gram representation is a frequency vector of operations, used in Nasbot [25]. When we use all $n \leq \ell$ where ℓ is the number of network

layers, the n -gram representation shares the same spirit as the path encoding, used in Bananas [62].

Let \mathbb{S} be the set of operations, and $\mathbb{S}^n = \mathbb{S} \times \mathbb{S} \times \dots \times \mathbb{S}$ (n times of \mathbb{S}), the n -gram can be represented as empirical measures in the followings

$$\omega_{\mathbf{x}}^o = \sum_{s \in \mathbb{S}^n} \mathbf{x}_s^o \delta_s, \quad \omega_{\mathbf{z}}^o = \sum_{s \in \mathbb{S}^n} \mathbf{z}_s^o \delta_s, \quad (3)$$

where \mathbf{x}_s^o and \mathbf{z}_s^o are the frequency of n -gram operation $s \in \mathbb{S}^n$ in architecture \mathbf{x} and \mathbf{z} , respectively.

We can leverage the TW distance to compare the n -gram representations $\omega_{\mathbf{x}}^o$ and $\omega_{\mathbf{z}}^o$ using Eq. (2), denoted as $W_{d_{\mathcal{T}_o}}(\omega_{\mathbf{x}}^o, \omega_{\mathbf{z}}^o)$. To compute this distance, we utilize a predefined tree structure for network operations by hierarchically grouping similar network operations into a tree as illustrated in Fig. 1. We can utilize the domain knowledge to define the grouping and the edge weights, such as we can have `conv1` and `conv3` in the same group and `maxpool` is from another group. Inspired by the partition-based tree metric sampling [30], we define the edge weights decreasing when the edge is far from the root. Although such design can be subjective, the final distance (defined later in Eq. (5)) will be calibrated and normalized properly when modeling with a GP in §3. We refer to Fig. 7 and Appendix §E for the example of TW computation for neural network architectures.

Indegree and outdegree representations for network structure. We extract the *indegree* and *outdegree* of each layer which are the number of ingoing and outgoing layers respectively, as an alternative way to represent a network structure. We denote $L_{\mathbf{x}}$ as the set of all layers which one can reach from the input layer for neural network \mathbf{x} . Let $\eta_{x,\ell}$ and M_x be lengths of the longest paths from the input layer to the layer ℓ and to the output layer respectively. Such paths interpret the order of layers in a neural network which starts with an input layer, connect with some middle layers, and end with an output layer, we represent the indegree and outdegree of network layers in \mathbf{x} as empirical measures $\omega_{\mathbf{x}}^{d-}$ and $\omega_{\mathbf{x}}^{d+}$, defined as

$$\omega_{\mathbf{x}}^{d-} = \sum_{\ell \in L_{\mathbf{x}}} \mathbf{x}_{\ell}^{d-} \delta_{\frac{\eta_{x,\ell}+1}{M_x+1}}, \quad \omega_{\mathbf{x}}^{d+} = \sum_{\ell \in L_{\mathbf{x}}} \mathbf{x}_{\ell}^{d+} \delta_{\frac{\eta_{x,\ell}+1}{M_x+1}}, \quad (4)$$

where \mathbf{x}_{ℓ}^{d-} and \mathbf{x}_{ℓ}^{d+} are the normalized indegree and outdegree of the layer ℓ of \mathbf{x} respectively.

For indegree and outdegree information, the supports of empirical measures $\omega_{\mathbf{x}}^{d-}$, and $\omega_{\mathbf{z}}^{d-}$ are in one-dimensional space that a tree structure reduces to a chain of supports. Thus, we can use $W_{d_{\mathcal{T}_-}}(\omega_{\mathbf{x}}^{d-}, \omega_{\mathbf{z}}^{d-})$ to compare those empirical measures². Similarly, we

have $W_{d_{\mathcal{T}_+}}(\omega_{\mathbf{x}}^{d+}, \omega_{\mathbf{z}}^{d+})$ for empirical measures $\omega_{\mathbf{x}}^{d+}$ and $\omega_{\mathbf{z}}^{d+}$ built from outdegree information.

Tree-Wasserstein distance for neural networks. Given neural networks \mathbf{x} and \mathbf{z} , we consider three separate TW distances for the n -gram, indegree and outdegree representations of the networks respectively. Then, we define d_{NN} as a convex combination with nonnegative weights $\{\alpha_1, \alpha_2, \alpha_3 \mid \sum_i \alpha_i = 1, \alpha_i \geq 0\}$ for $W_{d_{\mathcal{T}_o}}$, $W_{d_{\mathcal{T}_-}}$, and $W_{d_{\mathcal{T}_+}}$ respectively, to compare neural networks \mathbf{x} and \mathbf{z} as:

$$d_{\text{NN}}(\mathbf{x}, \mathbf{z}) = \alpha_1 W_{d_{\mathcal{T}_o}}(\mathbf{x}^o, \mathbf{z}^o) + \alpha_2 W_{d_{\mathcal{T}_-}}\left(\omega_{\mathbf{x}}^{d-}, \omega_{\mathbf{z}}^{d-}\right) + (1 - \alpha_1 - \alpha_2) W_{d_{\mathcal{T}_+}}\left(\omega_{\mathbf{x}}^{d+}, \omega_{\mathbf{z}}^{d+}\right). \quad (5)$$

The proposed discrepancy d_{NN} can capture not only frequency of layer operations, but also network structures, e.g., indegree and outdegree of network layers.

We illustrate our proposed TW for neural networks in Fig. 9 describing each component in Eq. (5). We also describe the detailed calculations in the Appendix §E. We highlight a useful property of our proposed d_{NN} : it can compare two architectures with *different* layer sizes and/or operations sizes.

Proposition 1. *The d_{NN} for neural networks is a pseudo-metric and negative definite.*

Proof of Proposition 1 is placed in the Appendix §D.2.

Our discrepancy d_{NN} is negative definite as opposed to the OT for neural networks considered in [25] which is indefinite. Therefore, from Proposition 1 and following Theorem 3.2.2 in [3], we can derive a positive definite TW kernel upon d_{NN} for neural networks \mathbf{x}, \mathbf{z} as

$$k(\mathbf{x}, \mathbf{z}) = \exp(-d_{\text{NN}}(\mathbf{x}, \mathbf{z})/\sigma_l^2), \quad (6)$$

where the scalar σ_l^2 is the length-scale parameter. Our kernel has three hyperparameters including a length-scale σ_l^2 in Eq. (6); α_1 and α_2 in Eq. (5). These hyperparameters will be estimated by maximizing the log marginal likelihood (see Appendix §F). We refer to the Appendix §G for further discussion about the properties of the pseudo-distance d_{NN} .

3 Neural Architecture Search with Gaussian Process and k-DPP

Problem setting. We consider a noisy black-box function $f : \mathbb{R}^d \rightarrow \mathbb{R}$ over some domain \mathcal{X} containing neural network architectures. As a black-box function, we do not have a closed-form for f and it is expensive to evaluate. Our goal is to find the best architecture

²Since the tree is a chain, the TW is equivalent to the univariate OT.

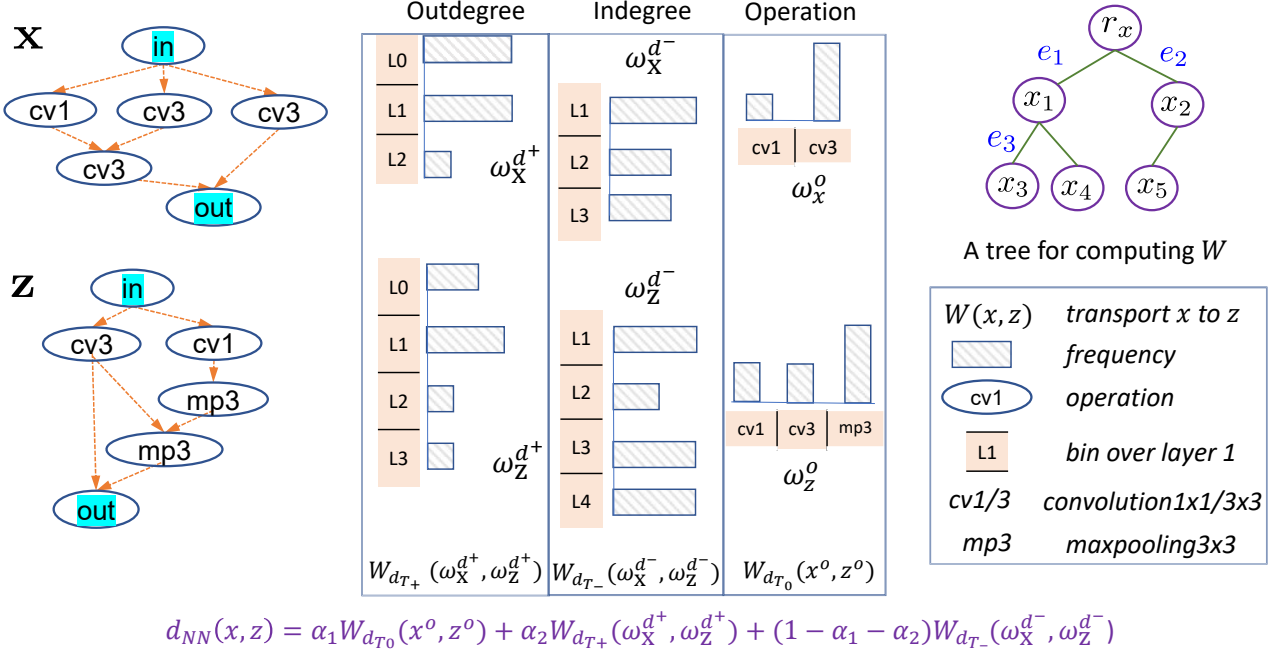


Figure 1: We represent two architectures \mathbf{x} and \mathbf{z} by network structure (via outdegree and indegree) and network operation (using 1-gram in this example). The similarity between each respective representation is estimated by tree-Wasserstein to compute the minimal cost of transporting one object to another. As a nice property of optimal transport, our tree-Wasserstein can handle *different* layer sizes and *different* operation types. The weights in each histogram are calculated from the architectures. The histogram bins in outdegree and indegree are aligned with the network structure in the left. See the Appendix §E for detailed calculations.

$\mathbf{x}^* \in \mathcal{X}$ such that

$$\mathbf{x}^* = \operatorname{argmax}_{\mathbf{x} \in \mathcal{X}} f(\mathbf{x}). \quad (7)$$

We view the black-box function above as a machine learning experiment which takes an input as a neural network architecture \mathbf{x} and produces an accuracy y . We can write $y = f(\mathbf{x}) + \epsilon$ where we have considered Gaussian noise $\epsilon \sim \mathcal{N}(0, \sigma_f^2)$ given the noise variance σ_f^2 estimated from the data.

Bayesian optimization (BO) optimizes the black-box function by sequentially evaluating the black-box function [19, 50, 37]. Particularly, BO can speed up the optimization process by using a probabilistic model to guide the search [52]. BO has demonstrated impressive success for optimising the expensive black-box functions across domains.

Surrogate models. Bayesian optimization reasons about f by building a surrogate model, such as a Gaussian process (GP) [43], Bayesian deep learning [54], deep neural network [53, 62] or random forest [5]. Among these choices, GP is the most popular model, offering three key benefits: (i) closed-form uncertainty estimation, (ii) evaluation efficiency, and (iii)

learning hyperparameters. A GP imposes a normally distributed random variable at every point in the input space. The predictive distribution for a new observation also follows a Gaussian distribution [43] where we can estimate the expected function value $\mu(\mathbf{x})$ and the predictive uncertainty $\sigma(\mathbf{x})$ as

$$\mu(\mathbf{x}') = \mathbf{k}(\mathbf{x}', \mathbf{X}) [\mathbf{K} + \sigma_f^2 \mathbf{I}]^{-1} \mathbf{y} \quad (8)$$

$$\sigma^2(\mathbf{x}') = k_{**} - \mathbf{k}(\mathbf{x}', \mathbf{X}) [\mathbf{K} + \sigma_f^2 \mathbf{I}]^{-1} \mathbf{k}^T(\mathbf{x}', \mathbf{X}) \quad (9)$$

where $\mathbf{X} = [\mathbf{x}_1, \dots, \mathbf{x}_N]$ and $\mathbf{y} = [y_1, \dots, y_N]$ are the collected architectures and performances; $K(U, V)$ is a covariance matrix whose element (i, j) is calculated as $k(\mathbf{x}_i, \mathbf{x}_j)$ with $\mathbf{x}_i \in U$ and $\mathbf{x}_j \in V$; $k_{**} = k(\mathbf{x}', \mathbf{x}')$; $\mathbf{K} := \mathbf{K}(\mathbf{X}, \mathbf{X})$; σ_f^2 is the measurement noise variance and \mathbf{I} is the identity matrix.

Generating a pool of candidates \mathcal{P}_t . We follow [25, 62] to generate a list of candidate networks using an evolutionary algorithm [1]. First, we stochastically select top-performing candidates with higher acquisition function values. Then, we apply a mutation operator to each candidate to produce modified architectures. Finally, we evaluate the acquisition on these mutations, add them to the initial pool, and repeat for several

steps to get a pool of candidates \mathcal{P}_t . We have the ablation study in Fig. 2 demonstrating that the evolution strategy outperforms the random strategy for this task.

Optimizing hyperparameters. We optimize the model hyperparameters by maximizing the log marginal likelihood. We present the derivatives for estimating the hyperparameters α_1 and α_2 of the tree-Wasserstein in the Appendix §F. We shall optimize these variables via multi-started gradient descent.

3.1 Sequential NAS using Bayes optimization

We sequentially suggest a *single* architecture for evaluation using a decision function $\alpha(\mathbf{x})$ (i.e., acquisition function) from the surrogate model. This acquisition function is carefully designed to trade off between exploration of the search space and exploitation of current promising regions. We utilize the GP-UCB [55] as the main decision function $\alpha(\mathbf{x}) = \mu(\mathbf{x}) + \kappa\sigma(\mathbf{x})$ where κ is the parameter controlling the exploration, μ and σ are the GP predictive mean and variance in Eqs. (8,9). Empirically, we find that this GP-UCB generally performs better than expected improvement (EI) (see the Appendix §H.1) and other acquisition functions (see [62]). We note that the GP-UCB also comes with a theoretical guarantee for convergence [55].

We maximize the acquisition function to select the next architecture $\mathbf{x}_{t+1} = \arg \max_{\mathbf{x} \in \mathcal{P}_t} \alpha_t(\mathbf{x})$. This maximization is done on the discrete set of candidate \mathcal{P}_t obtained previously. The selected candidate is the one we expect to be the best if we are optimistic in the presence of uncertainty.

3.2 Parallel NAS using Quality k-DPP and Gaussian Process

The parallel setting speeds up the optimization process by selecting a *batch* of architectures for parallel evaluations. We present the k-determinantal point process (k-DPP) with *quality* to select from a discrete pool of candidate \mathcal{P}_t for (i) high-performing and (ii) diverse architectures that cover the most information while avoiding redundancy. In addition, diversity is an important property for not being stuck at a local optimal architecture.

The DPP [29] is an elegant probabilistic measure used to model negative correlations within a subset and hence promote its diversity. A k-determinantal point process (k-DPP) [28] is a distribution over all subsets of a ground set \mathcal{P}_t of cardinality k. It is determined by a positive semidefinite kernel $\mathbf{K}_{\mathcal{P}_t}$. Let \mathbf{K}_A be the submatrix of $\mathbf{K}_{\mathcal{P}_t}$ consisting of the entries \mathbf{K}_{ij} with $i, j \in A \subseteq \mathcal{P}_t$. Then, the probability of observing $A \subseteq \mathcal{P}_t$ is proportional to $\det(\mathbf{K}_A)$,

Algorithm 1 Sequential and Parallel NAS using Gaussian process with tree-Wasserstein kernel

```

1: Input: Initial data  $\mathcal{D}_0$ , black-box function  $f(\mathbf{x})$ .
   Output: The best architecture  $\mathbf{x}^*$ 
2: for  $t = 1, \dots, T$  do
3:   Generate architecture candidates  $\mathcal{P}_t$  by random
      permutation from the top architectures.
4:   Learn a GP (including hyperparameters) using
      TW from  $\mathcal{D}_{t-1}$  to perform estimation over  $\mathcal{P}_t$  in-
      cluding (i) covariance matrix  $\mathbf{K}_{\mathcal{P}_t}$ , (ii) predictive
      mean  $\mu_{\mathcal{P}_t}$  and (iii) predictive variance  $\sigma_{\mathcal{P}_t}$ 
5:   If Sequential: select a next architecture  $\mathbf{x}_t =$ 
      
$$\underset{\mathbf{x} \in \mathcal{P}_t}{\operatorname{argmax}} \alpha(\mathbf{x} | \mu_{\mathcal{P}_t}, \sigma_{\mathcal{P}_t})$$

6:   Evaluate the new architecture  $y_t = f(\mathbf{x}_t)$ 
7:   Augment  $\mathcal{D}_t \leftarrow \mathcal{D}_{t-1} \cup (\mathbf{x}_t, y_t)$ 
8:   If Parallel: select  $B$  architectures  $\mathbf{X}_t =$ 
      
$$[\mathbf{x}_{t,1}, \dots, \mathbf{x}_{t,B}] = \text{k-DPP}(\mathbf{K}_{\mathcal{P}_t})$$
 in Eq. (12)
9:   Evaluate in parallel  $Y_t = f(\mathbf{X}_t)$ 
10:  Augment  $\mathcal{D}_t \leftarrow \mathcal{D}_{t-1} \cup (\mathbf{X}_t, Y_t)$ 
11: end for

```

$$P(A \subseteq \mathcal{P}_t) \propto \det(\mathbf{K}_A), \quad (10) \quad \mathbf{K}_{ij} = q_i \phi_i^T \phi_i q_j. \quad (11)$$

k-DPP with quality. While the original idea of a k-DPP is to find a diverse subset, we can extend it to find a subset which is both diverse and high-quality. For this, we write a DPP kernel k as a Gram matrix, $\mathbf{K} = \Phi^T \Phi$, where the columns of Φ are vectors representing items in the set S . We now take this one step further, writing each column Φ as the product of a quality term $q_i \in \mathcal{R}^+$ and a vector of normalized diversity features ϕ_i , $\|\phi_i\| = 1$. The entries of the kernel can now be written in Eq. (11).

As discussed in [29], this decomposition of \mathbf{K} has two main advantages. First, it implicitly enforces the constraint that \mathbf{K} must be positive semidefinite, which can potentially simplify learning. Second, it allows us to independently model quality and diversity, and then combine them into a unified model. Particularly, we have $P_K(A) \propto (\prod_{i \in A} q_i^2) \det(\phi_i^T \phi_i)$ where the first term increases with the quality of the selected items, and the second term increases with the diversity of the selected items. Without the quality component, we would get a very diverse set of architectures, but we might fail to include the most high-performance architectures in \mathcal{P}_t , focusing instead on low-quality outliers. By integrating the two models we can achieve a more balanced result.

Conditioning. In the parallel setting, given the training data, we would like to select high quality and diverse architectures from a pool of candidate \mathcal{P}_t de-

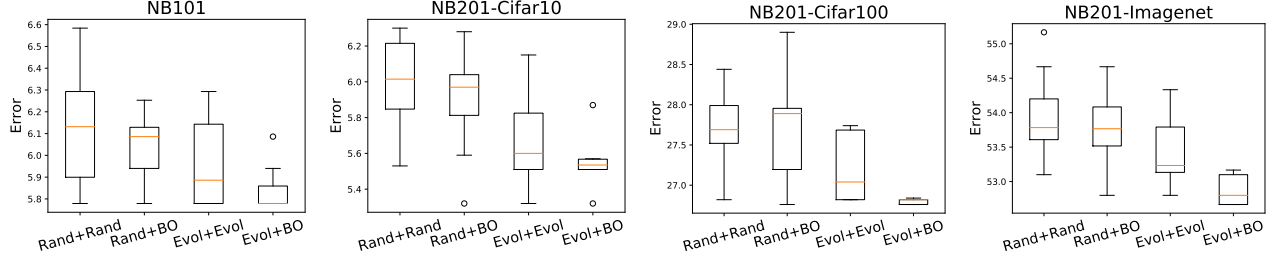


Figure 2: We study the relative contribution of the strategies generating a pool of candidate \mathcal{P} (Rand and Evolution) versus the main optimization algorithm (Rand, Evolution and BO). The result shows that Evolution can help to improve the performance than Rand in generating a pool of candidate \mathcal{P} . Given the same strategy for generating \mathcal{P} , BO is significantly better than Rand and Evolution for optimization. Evol+BO is the design in our approach that leads to the best performance.

scribed above. We shall condition on the training data in constructing the covariance matrix over the testing candidates from \mathcal{P}_t . We make the following proposition in connecting the k-DPP conditioning and GP uncertainty estimation. This view allows us to learn the covariance matrix using GP, such as we can maximize the GP marginal likelihood for learning the TW distance and kernel hyperparameters for k-DPP.

Proposition 2. *Conditioned on the training set, the probability of selecting new candidates from a pool \mathcal{P}_t is equivalent to the determinant of the Gaussian process predictive covariance matrix.*

Proof of Proposition 2 is placed in the Appendix §F.1.

We can utilize the GP predictive mean $\mu(\cdot)$ in Eq. (8) to estimate the quality for any unknown architecture q_i defined in Eq. (11). Then, we construct the covariance (kernel) matrix over the test candidates for selection by rewriting Eq. (11) as

$$\mathbf{K}_{\mathcal{P}_t}(\mathbf{x}_i, \mathbf{x}_j) = \exp(-\mu(\mathbf{x}_i)) \sigma(\mathbf{x}_i, \mathbf{x}_j) \exp(-\mu(\mathbf{x}_j)) \quad (12)$$

$\forall \mathbf{x}_i, \mathbf{x}_j \in \mathcal{P}_t$ where $\mu(\mathbf{x}_i)$ and $\sigma(\mathbf{x}_i, \mathbf{x}_j)$ are the GP predictive mean and variance defined in Eqs. (8,9). Each term in Eq. (12) are naturally in range $[0, 1]$, thus it balances between diversity and quality. Finally, we sample B architectures from the covariance matrix $\mathbf{K}_{\mathcal{P}_t}$ which encodes both the diversity (exploration) and high-utility (exploitation). The sampling algorithm requires precomputing the eigenvalues [28]. Sampling from a k-DPP requires $\mathcal{O}(NB^2)$ time overall where B is the batch size.

Advantages. The connection between GP and k-DPP allows us to directly sample diverse and high-quality samples from the GP posterior. This leads to the key advantage that we can *optimally* sample a batch of candidates without the need of greedy selection. On the other hand, the existing batch BO approaches rely either on greedy strategy [7, 8, 21] to sequentially

select the points in a batch or independent sampling [15, 23]. The greedy algorithm is non-optimal and the independent sampling approaches can not fully utilize the information across points in a batch.

We note that our k-DPP above is related to [26], but different from two perspectives that [26] considers k-DPP for batch BO in the (i) continuous setting and (ii) using pure exploration (without quality). We will consider this as the baseline in the experiment.

4 Experiments

Experimental settings. All experimental results are averaged over 30 independent runs with different random seeds. We set the number of candidate architecture in each $|\mathcal{P}_t| = 100$. We attach all source codes with the submission and will release them in the final version. We utilize the popular NAS tabular datasets of Nasbench101 (NB101) [66] and Nasbench201 (NB201) [11] for evaluations. TW and TW-2G stand for our TW using 1-gram and 2-gram representation respectively.

4.1 Sequential NAS

Ablation study: different mechanism for generating a pool of candidates \mathcal{P} . We analyze the relative contribution of the process of generating architecture candidates versus the main optimization algorithm in Fig. 2. The result suggests that the evolutionary algorithm is better than random strategy to generate a pool of candidates \mathcal{P} . Given this generated candidate set \mathcal{P} , BO is significantly better than Rand and Evolution approaches. In brief, the combination of Evol+BO performs the best across datasets.

Ablation study: different distances for BO. We design an ablation study using different distances within a BO framework. Particularly, we consider the vanilla optimal transport (Wasserstein distance)

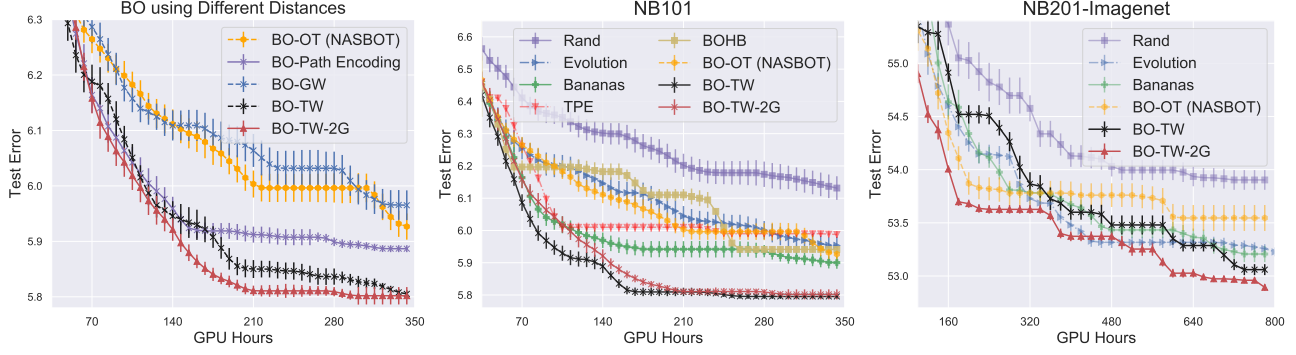


Figure 3: Sequential NAS on different distances for BO (left) and different baselines (middle and right). Our approaches of BO-TW (black curve) and BO-TW 2G (red curve) for 1-gram and 2-gram representation consistently outperform the other baselines. We use 500 iterations on NB101 and 200 iterations on NB201.

in which we follow [25] to define the cost metric for OT. This baseline can be seen as the modified version of the Nasbot [25]. In addition, we compare our approach with the BO using the Gromov-Wasserstein distance [35] (BO-GW) and path encoding (BO-Path Encoding) as used in [62]. The results in Left Fig. 3 suggest that the proposed TW using 2-gram performs the best among the BO distance for neural network architectures. The OT and GW will result in (non-p.s.d.) indefinite kernels. For using OT and GW in our GP, we keep adding (“jitter”) noise to the diagonal of the kernel matrices until they become p.s.d. kernels. We make use of the POT library [16] for the implementation of OT and GW.

While our framework is able to handle n -gram representation, we learn that 2-gram is empirically the best choice. This choice is well supported by the fact that two convolution layers of 3×3 stay together can be used to represent for a special effect of 5×5 convolution kernel. In addition, the use of full n -gram may result in very sparse representation and some features are not so meaningful anymore. Therefore, in the experiment we only consider 1-gram and 2-gram.

Sequential NAS. We validate our GP-BO model using tree-Wasserstein on the sequential setting. Since NB101 is somewhat harder than NB201, we allocate 500 queries for NB101 and 200 queries for NB201 including 10% of random selection at the beginning of BO.

We compare our approach against the common baselines including Random search, evolutionary search, TPE [4], BOHB [15], Nasbot [25] and Bananas [62]. We use the AutoML library for TPE and BOHB³ including the results for NB101, but not NB201. We do not compare with Reinforcement Learning approaches [40] and AlphaX [60] which have been shown to perform poorly in [62].

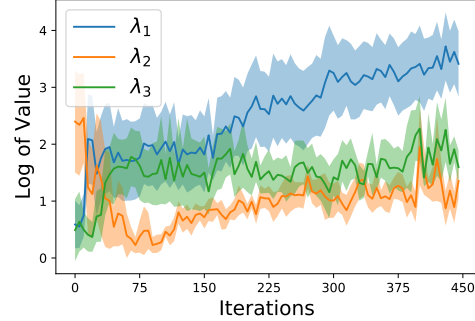


Figure 4: Estimated hyperparameters on NB101.

We show in Fig. 3 that our tree-Wasserstein including 1-gram and 2-gram will result in the best performance with a wide margin to the second best – a Bananas [62], which needs to specify the meta neural network with extra hyperparameters (layers, nodes, learning rate). The random search performs poorly in NAS due to the high-dimensional and complex space. Our GP-based optimizer offers a closed-form uncertainty estimation without iterative approximation in neural network (via back-propagation). As a property of GP, our BO-TW can generalize well using fewer observations. This can be seen in Right Fig. 3 that our approaches can outperform Bananas when the number of BO iteration (or number of architecture for training) is small. On the other hand, both Bananas and ours are converging to the same performance when the training data becomes abundant – but this is not the case in practice for NAS.

Estimating hyperparameters. We plot the estimated hyperparameters $\lambda_1 = \frac{\alpha_1}{\sigma_1^2}$, $\lambda_2 = \frac{\alpha_2}{\sigma_2^2}$, $\lambda_3 = \frac{1-\alpha_1-\alpha_2}{\sigma_3^2}$ over iterations in Fig. 4. This indicates the relative contribution of the operation, indegree and outdegree toward the d_{NN} in Eq. (5). Particularly, the operation contributes receives more weight and is useful information than the individual indegree or outdegree.

³https://github.com/automl/nas_benchmarks

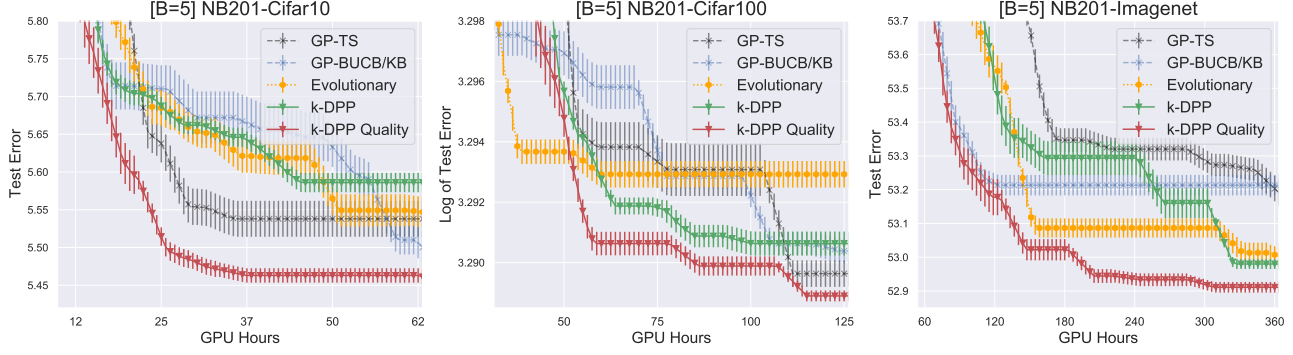


Figure 5: Batch NAS comparison using TW-2Gram and a batch size $B = 5$. Our proposed k-DPP Quality (red) outperforms other baselines in all cases, especially when the number of training architecture (iterations) is low. This is the desirable property of NAS when the training cost is extremely expensive. The experiments are run over 100 iterations.

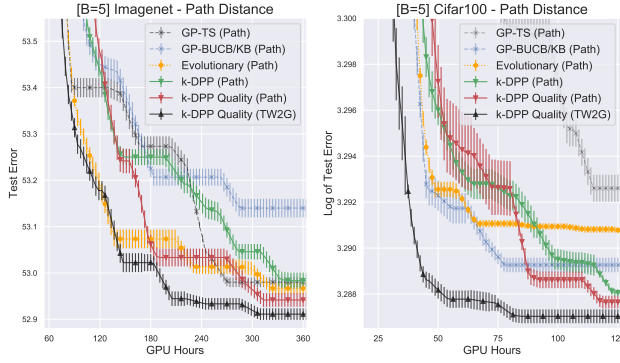


Figure 6: We compare different batch approaches using a path distance [62] and a batch size $B = 5$. We show that (1) the k-DPP quality outperforms the other batch approaches and (2) the k-DPP using TW2G (a black curve) performs better than using path distance (a red curve).

4.2 Batch NAS

We next demonstrate our model on selecting multiple architectures for parallel evaluation–parallel NAS setting. There are fewer approaches for parallel NAS compared to the sequential setting. We select to compare our k-DPP quality against Thompson sampling [23], GP-BUCB [8] and k-DPP for batch BO [26]. The GP-BUCB is equivalent to Krigging believer [20] when the hallucinated observation value is set to the GP predictive mean. Therefore, we label them as GP-BUCB/KB. We also compare with the vanilla k-DPP (without using quality) [26].

We allocate a maximum budget of 500 queries including 50 random initial architectures. The result in Fig. 5 shows that our proposed k-DPP quality is the best among the baselines. We refer to the Appendix for additional experiments including varying batch sizes and more results on NB201.

Our sampling from k-DPP quality is advantageous against the existing batch BO approaches [20, 8, 26, 23] in that we can optimally select a batch of architectures without relying on the greedy selection strategy. In addition, our k-DPP quality can leverage the benefit of the GP in estimating the hyperparameters for the covariance matrix.

Ablation study of k-DPP quality with path distance. Additional to the proposed tree-Wasserstein, we demonstrate the proposed k-DPP quality using path distance [62]. We show that our k-DPP quality is not restricted to TW-2G, but it can be generally used with different choices of kernel distances.

Particularly, we present in Fig. 6 the comparison using two datasets: Imagenet and Cifar100 in NB201. The results validate two messages as follows. First, our k-DPP quality is the best among the other baselines in selecting high-performing and diverse architectures. Second, our k-DPP quality with TW2G (a black curve) performs better than k-DPP quality using Path distance (a red curve). This demonstrates the key benefits of comparing two complex architectures as logistical supplier and receiver.

5 Conclusion

We have presented a new framework for sequential and parallel NAS. Our framework constructs the similarity between architectures using tree-Wasserstein geometry. Then, it utilizes the Gaussian process surrogate for modeling and optimization. We draw the connection between GP predictive distribution to k-DPP quality for selecting diverse and high-performing architectures from discrete set. We demonstrate our model using Nasbench101 and Nasbench201 that our methods outperform the existing baselines in sequential and parallel settings.

References

- [1] Thomas Back. *Evolutionary algorithms in theory and practice: evolution strategies, evolutionary programming, genetic algorithms*. Oxford university press, 1996.
- [2] Bowen Baker, Otkrist Gupta, Nikhil Naik, and Ramesh Raskar. Designing neural network architectures using reinforcement learning. *International Conference on Learning Representations*, 2017.
- [3] Christian Berg, Jens Peter Reus Christensen, and Paul Ressel. *Harmonic analysis on semigroups*. Springer-Verlag, 1984.
- [4] J S Bergstra, R Bardenet, Y Bengio, and B Kégl. Algorithms for hyper-parameter optimization. In *Advances in Neural Information Processing Systems*, pages 2546–2554, 2011.
- [5] Leo Breiman. Random forests. *Machine learning*, 45(1):5–32, 2001.
- [6] Rainer E Burkard and Eranda Cela. Linear assignment problems and extensions. In *Handbook of combinatorial optimization*, pages 75–149. Springer, 1999.
- [7] Emile Contal, David Buffoni, Alexandre Robicquet, and Nicolas Vayatis. Parallel gaussian process optimization with upper confidence bound and pure exploration. In *Machine Learning and Knowledge Discovery in Databases*, pages 225–240. Springer, 2013.
- [8] Thomas Desautels, Andreas Krause, and Joel W Burdick. Parallelizing exploration-exploitation tradeoffs in gaussian process bandit optimization. *The Journal of Machine Learning Research*, 15(1):3873–3923, 2014.
- [9] Khanh Do Ba, Huy L Nguyen, Huy N Nguyen, and Ronitt Rubinfeld. Sublinear time algorithms for Earth Mover’s distance. *Theory of Computing Systems*, 48(2):428–442, 2011.
- [10] Xuanyi Dong and Yi Yang. Searching for a robust neural architecture in four gpu hours. In *Proceedings of the IEEE Conference on Computer Vision and Pattern Recognition*, pages 1761–1770, 2019.
- [11] Xuanyi Dong and Yi Yang. Nas-bench-201: Extending the scope of reproducible neural architecture search. *International Conference on Learning Representation*, 2020.
- [12] Thomas Elsken, Jan Hendrik Metzen, and Frank Hutter. Efficient multi-objective neural architecture search via lamarckian evolution. *International Conference on Learning Representation*, 2019.
- [13] Thomas Elsken, Jan Hendrik Metzen, and Frank Hutter. Neural architecture search: A survey. *Journal of Machine Learning Research*, 20(55):1–21, 2019.
- [14] Steven N Evans and Frederick A Matsen. The phylogenetic Kantorovich–Rubinstein metric for environmental sequence samples. *Journal of the Royal Statistical Society: Series B (Statistical Methodology)*, 74(3):569–592, 2012.
- [15] Stefan Falkner, Aaron Klein, and Frank Hutter. Bohb: Robust and efficient hyperparameter optimization at scale. In *International Conference on Machine Learning*, pages 1436–1445, 2018.
- [16] Rémi Flamary and Nicolas Courty. Pot python optimal transport library. *GitHub*: <https://github.com/rflamary/POT>, 2017.
- [17] Peter I Frazier. A tutorial on Bayesian optimization. *arXiv preprint arXiv:1807.02811*, 2018.
- [18] Xinbo Gao, Bing Xiao, Dacheng Tao, and Xuelong Li. A survey of graph edit distance. *Pattern Analysis and applications*, 13(1):113–129, 2010.
- [19] Roman Garnett, Michael A Osborne, and Stephen J Roberts. Bayesian optimization for sensor set selection. In *Proceedings of the 9th ACM/IEEE international conference on information processing in sensor networks*, pages 209–219, 2010.
- [20] David Ginsbourger, Rodolphe Le Riche, and Laurent Carraro. Kriging is well-suited to parallelize optimization. In *Computational Intelligence in Expensive Optimization Problems*, pages 131–162. Springer, 2010.
- [21] Javier González, Zhenwen Dai, Philipp Hennig, and Neil D Lawrence. Batch Bayesian optimization via local penalization. In *International Conference on Artificial Intelligence and Statistics*, pages 648–657, 2016.
- [22] Shivaprata Gopakumar, Sunil Gupta, Santu Rana, Vu Nguyen, and Svetha Venkatesh. Algorithmic assurance: An active approach to algorithmic testing using Bayesian optimisation. In *Advances in Neural Information Processing Systems*, pages 5465–5473, 2018.

- [23] José Miguel Hernández-Lobato, James Requeima, Edward O Pyzer-Knapp, and Alán Aspuru-Guzik. Parallel and distributed Thompson sampling for large-scale accelerated exploration of chemical space. In *International Conference on Machine Learning*, pages 1470–1479, 2017.
- [24] Haifeng Jin, Qingquan Song, and Xia Hu. Auto-keras: Efficient neural architecture search with network morphism. 2018.
- [25] Kirthevasan Kandasamy, Willie Neiswanger, Jeff Schneider, Barnabas Poczos, and Eric P Xing. Neural architecture search with bayesian optimisation and optimal transport. In *Advances in Neural Information Processing Systems*, pages 2016–2025, 2018.
- [26] Tarun Kathuria, Amit Deshpande, and Pushmeet Kohli. Batched Gaussian process bandit optimization via determinantal point processes. In *Advances in Neural Information Processing Systems*, pages 4206–4214, 2016.
- [27] R Kondor and J Lafferty. Diffusion kernels on graphs and other discrete input spaces. In *International Conference on Machine Learning*, pages 315–322, 2002.
- [28] Alex Kulesza and Ben Taskar. k-dpps: Fixed-size determinantal point processes. In *Proceedings of the 28th International Conference on Machine Learning*, pages 1193–1200, 2011.
- [29] Alex Kulesza, Ben Taskar, et al. Determinantal point processes for machine learning. *Foundations and Trends® in Machine Learning*, 5(2–3):123–286, 2012.
- [30] Tam Le, Makoto Yamada, Kenji Fukumizu, and Marco Cuturi. Tree-sliced variants of Wasserstein distances. In *Advances in Neural Information Processing Systems*, pages 12283–12294, 2019.
- [31] Lisha Li and Kevin Jamieson. Hyperband: A novel bandit-based approach to hyperparameter optimization. *Journal of Machine Learning Research*, 18:1–52, 2018.
- [32] Hanxiao Liu, Karen Simonyan, Oriol Vinyals, Chrisantha Fernando, and Koray Kavukcuoglu. Hierarchical representations for efficient architecture search. *International Conference on Learning Representation*, 2018.
- [33] Hanxiao Liu, Karen Simonyan, and Yiming Yang. Darts: Differentiable architecture search. *International Conference on Learning Representation*, 2019.
- [34] Renqian Luo, Fei Tian, Tao Qin, Enhong Chen, and Tie-Yan Liu. Neural architecture optimization. In *Advances in Neural Information Processing Systems*, pages 7816–7827, 2018.
- [35] Facundo Mémoli. Gromov–wasserstein distances and the metric approach to object matching. *Foundations of computational mathematics*, 11(4):417–487, 2011.
- [36] Bruno T Messmer and Horst Bunke. A new algorithm for error-tolerant subgraph isomorphism detection. *IEEE transactions on pattern analysis and machine intelligence*, 20(5):493–504, 1998.
- [37] Vu Nguyen and Michael A Osborne. Knowing the what but not the where in Bayesian optimization. In *International Conference on Machine Learning*, 2020.
- [38] Vu Nguyen, Sebastian Schulze, and Michael A Osborne. Bayesian optimization for iterative learning. In *Advances in Neural Information Processing Systems*, 2020.
- [39] Gabriel Peyré and Marco Cuturi. Computational optimal transport. *Foundations and Trends in Machine Learning*, 11(5–6):355–607, 2019.
- [40] Hieu Pham, Melody Guan, Barret Zoph, Quoc Le, and Jeff Dean. Efficient neural architecture search via parameters sharing. In *International Conference on Machine Learning*, pages 4095–4104, 2018.
- [41] Ali Rahimi and Benjamin Recht. Random features for large-scale kernel machines. In *Advances in Neural Information Processing Systems*, pages 1177–1184, 2007.
- [42] Santu Rana, Cheng Li, Sunil Gupta, Vu Nguyen, and Svetha Venkatesh. High dimensional Bayesian optimization with elastic Gaussian process. In *Proceedings of the 34th International Conference on Machine Learning*, pages 2883–2891, 2017.
- [43] Carl Edward Rasmussen. Gaussian processes for machine learning. 2006.
- [44] Esteban Real, Alok Aggarwal, Yanping Huang, and Quoc V Le. Regularized evolution for image classifier architecture search. In *Proceedings of the AAAI conference on Artificial Intelligence*, volume 33, pages 4780–4789, 2019.
- [45] Esteban Real, Sherry Moore, Andrew Selle, Saurabh Saxena, Yutaka Leon Suematsu, Jie Tan, Quoc V Le, and Alexey Kurakin. Large-scale evolution of image classifiers. In *Proceedings of the 34th International Conference on Machine Learning*, pages 2902–2911, 2017.

- [46] Binxin Ru, Ahsan S Alvi, Vu Nguyen, Michael A Osborne, and Stephen J Roberts. Bayesian optimisation over multiple continuous and categorical inputs. In *International Conference on Machine Learning*, 2020.
- [47] Christian Sciuto, Kaicheng Yu, Martin Jaggi, Claudiu Musat, and Mathieu Salzmann. Evaluating the search phase of neural architecture search. *arXiv preprint arXiv:1902.08142*, 2019.
- [48] Charles Semple and Mike Steel. Phylogenetics. *Oxford Lecture Series in Mathematics and its Applications*, 2003.
- [49] Syed Asif Raza Shah, Wenji Wu, Qiming Lu, Liang Zhang, Sajith Sasidharan, Phil DeMar, Chin Guok, John Macauley, Eric Pouyoul, Jin Kim, et al. Amoebanet: An sdn-enabled network service for big data science. *Journal of Network and Computer Applications*, 119:70–82, 2018.
- [50] Bobak Shahriari, Kevin Swersky, Ziyu Wang, Ryan P Adams, and Nando de Freitas. Taking the human out of the loop: A review of Bayesian optimization. *Proceedings of the IEEE*, 104(1):148–175, 2016.
- [51] Alexander J Smola and Risi Kondor. Kernels and regularization on graphs. In *Learning theory and kernel machines*, pages 144–158. Springer, 2003.
- [52] Jasper Snoek, Hugo Larochelle, and Ryan P Adams. Practical Bayesian optimization of machine learning algorithms. In *Advances in Neural Information Processing Systems*, pages 2951–2959, 2012.
- [53] Jasper Snoek, Oren Rippel, Kevin Swersky, Ryan Kiros, Nadathur Satish, Narayanan Sundaram, Mostofa Patwary, Mr Prabhat, and Ryan Adams. Scalable Bayesian optimization using deep neural networks. In *Proceedings of the 32nd International Conference on Machine Learning*, pages 2171–2180, 2015.
- [54] Jost Tobias Springenberg, Aaron Klein, Stefan Falkner, and Frank Hutter. Bayesian optimization with robust bayesian neural networks. In *Advances in Neural Information Processing Systems*, pages 4134–4142, 2016.
- [55] Niranjan Srinivas, Andreas Krause, Sham Kakade, and Matthias Seeger. Gaussian process optimization in the bandit setting: No regret and experimental design. In *Proceedings of the 27th International Conference on Machine Learning*, pages 1015–1022, 2010.
- [56] Masanori Suganuma, Shinichi Shirakawa, and Tomoharu Nagao. A genetic programming approach to designing convolutional neural network architectures. In *Proceedings of the Genetic and Evolutionary Computation Conference*, pages 497–504, 2017.
- [57] Cedric Villani. *Topics in optimal transportation*. American Mathematical Soc., 2003.
- [58] S Vichy N Vishwanathan, Nicol N Schraudolph, Risi Kondor, and Karsten M Borgwardt. Graph kernels. *Journal of Machine Learning Research*, 11(Apr):1201–1242, 2010.
- [59] Walter D Wallis, Peter Shoubridge, M Kraetz, and D Ray. Graph distances using graph union. *Pattern Recognition Letters*, 22(6-7):701–704, 2001.
- [60] Linnan Wang, Yiyang Zhao, Yuu Jinmai, Yuan-dong Tian, and Rodrigo Fonseca. Alphax: exploring neural architectures with deep neural networks and monte carlo tree search. *The Thirty-Fourth AAAI Conference on Artificial Intelligence*, 2020.
- [61] Zi Wang, Clement Gehring, Pushmeet Kohli, and Stefanie Jegelka. Batched large-scale Bayesian optimization in high-dimensional spaces. In *International Conference on Artificial Intelligence and Statistics*, pages 745–754, 2018.
- [62] Colin White, Willie Neiswanger, and Yash Savani. Bananas: Bayesian optimization with neural architectures for neural architecture search. *arXiv preprint arXiv:1910.11858*, 2019.
- [63] Lingxi Xie and Alan Yuille. Genetic cnn. In *Proceedings of the IEEE International Conference on Computer Vision*, pages 1379–1388, 2017.
- [64] Sirui Xie, Hehui Zheng, Chunxiao Liu, and Liang Lin. Snas: stochastic neural architecture search. *International Conference on Learning Representation*, 2019.
- [65] Quanming Yao, Ju Xu, Wei-Wei Tu, and Zhanxing Zhu. Efficient neural architecture search via proximal iterations. In *AAAI Conference on Artificial Intelligence*, 2020.
- [66] Chris Ying, Aaron Klein, Eric Christiansen, Esteban Real, Kevin Murphy, and Frank Hutter. Nas-bench-101: Towards reproducible neural architecture search. In *International Conference on Machine Learning*, pages 7105–7114, 2019.
- [67] Zhao Zhong, Junjie Yan, Wei Wu, Jing Shao, and Cheng-Lin Liu. Practical block-wise neural network architecture generation. In *Proceedings of the IEEE conference on Computer Vision and Pattern Recognition*, pages 2423–2432, 2018.

- [68] Barret Zoph and Quoc V Le. Neural architecture search with reinforcement learning. *International Conference on Representation Learning*, 2017.

Supplementary Material for: Optimal Transport Kernels for Sequential and Parallel Neural Architecture Search

In this appendix, we first review the related approaches in sequential and batch neural architecture search. We then present the illustrative example of the proposed tree-Wasserstein distance for neural network architecture. Then, we provide additional details of the Bayesian optimization in estimating the hyperparameters. Finally, we show further empirical comparisons and analysis for the model.

A Related works in Neural architecture search

We refer the interested readers to the survey paper [13] and the literature of neural architecture search⁴ for the comprehensive survey on neural architecture search. Many different search strategies have been attempted to explore the space of neural architectures, including random search, evolutionary methods, reinforcement learning (RL), gradient-based methods and Bayesian optimization.

Evolutionary approaches. [45, 44, 56, 32, 49, 63, 12] have been extensively used for NAS. In the context of evolutionary evolving, the mutation operations include adding a layer, removing a layer or changing the type of a layer (e.g., from convolution to pooling) from the neural network architecture. Then, the evolutionary approaches will update the population, e.g., tournament selection by removing the worst or oldest individual from a population.

Reinforcement learning. NASNet [68] is a reinforcement learning algorithm for NAS which achieves state-of-the-art results on CIFAR-10 and PTB; however, the algorithm requires 3000 GPU days to train. Efficient Neural Architecture Search (ENAS) [40] proposes to use a controller which discovers architectures by learning to search for an optimal subgraph within a large graph. The controller is trained with policy gradient to select a subgraph that maximizes the validation set's expected reward. The model corresponding to the subgraph is trained to minimize a canonical cross entropy loss. Multiple child models share parameters, ENAS requires fewer GPU-hours than other approaches and 1000-fold less than "standard" NAS. Other reinforcement learning approaches for NAS have also proposed, such as MetaQNN [2] and BlockQNN [67].

Gradient-based approaches. [34, 33, 10, 65] represent the search space as a directed acyclic graph (DAG) containing billions of sub-graphs, each of which indicates a kind of neural architecture. To avoid traversing all the possibilities of the sub-graphs, they develop a differentiable sampler over the DAG. The benefit of such idea is that a differentiable space enables computation of gradient information, which could speed up the convergence of underneath optimization algorithm. Various techniques have been proposed, e.g., DARTS [33], SNAS [64], and NAO [34]. While these approaches based on gradient-based learning can reduce the computational resources required for NAS, it is currently not well understood if an initial bias in exploring certain parts of the search space more than others might lead to the bias and thus result in premature convergence of NAS [47]. In addition, the gradient-based approach may be less appropriate for exploring different space (e.g., with completely different number of layers), as opposed to the approach presented in this paper.

Bayesian optimization. BO has been an emerging technique for black-box optimization when function evaluations are expensive [42, 17, 22], and it has seen great success in hyperparameter optimization for deep learning [31, 38, 46]. Recently, Bayesian optimization has been used for searching the best neural architecture [25, 24, 62]. BO relies on a covariance function to represent the similarity between two data points. For such similarity representation, we can (1) directly measure the similarity of the networks by optimal transport, then modeling with GP surrogate in [25]; or (2) measure the graphs based on the path-based encodings, then modeling with neural network surrogate in [62]. OTMANN [25] shares similarities with Wasserstein (earth mover's) distances which also have an OT formulation. However, it is not a Wasserstein distance itself—in particular, the supports of the masses and the cost matrices change depending on the two networks being compared. One of the drawback of OTMANN is that it may not be negative definite for a p.s.d. kernel which is an important requirement for modeling with GP. This is the motivation for our proposed tree-Wasserstein.

⁴<https://www.automl.org/automl/literature-on-neural-architecture-search>

Path-based encoding. Bananas [62] proposes the path-based encoding for neural network architectures. The drawback of path-based encoding is that we need to enumerate all possible paths from the input node to the output node, in terms of the operations. This can potentially raise although it can work well in NASBench dataset [66] which results in $\sum_{i=0}^5 3^i = 364$ possible paths.

Kernel graph. Previous work considers the neural network architectures as the graphs, then defining various distances and kernels on graphs [18, 27, 36, 51, 59]. However, they may not be ideal for our NAS setting because neural networks have additional complex properties in addition to graphical structure, such as the type of operations performed at each layer, the number of neurons, etc. Some methods do allow different vertex sets [58], they cannot handle layer masses and layer similarities.

B Related works in batch neural architecture search

There are several approaches in the literature which can be used to select multiple architectures for evaluation, including monte carlo tree search [60], evolutionary search [44] and most of the batch Bayesian optimization approaches, such as Kriging believer [20], GP-BUCB [8], GP-Thompson Sampling [23], and BOHB [15].

Kriging believer (KB) [20] exploits an interesting fact about GPs: the predictive variance of GPs depends only on the input x , but not the outcome values y . KB will iteratively construct a batch of points. First, it finds the maximum of the acquisition function, like the sequential setting. Next, KB moves to the next maximum by suppressing this point. This is done by inserting the outcome at this point as a halucinated value. This process is repeated until the batch is filled.

GP-BUCB [8] is related to the above Kriging believer in exploiting the GP predictive variance. Particularly, GP-BUCB is similar to KB when the halucinated value is set to the GP predictive mean.

GP-Thompson Sampling [23] generates a batch of points by drawing from the posterior distribution of the GP to fill in a batch. In the continuous setting, we can draw a GP sample using random Fourier feature [41]. In our discrete case of NAS, we can simply draw samples from the GP predictive mean.

C Datasets

We summarize two benchmark datasets used in the paper. Neural architecture search (NAS) methods are notoriously difficult to reproduce and compare due to different search spaces, training procedures and computing cost. These make methods inaccessible to most researchers. Therefore, the below two benchmark datasets have been created.

NASBENCH101. The NAS-Bench-101 dataset⁵ contains over 423,000 neural architectures with precomputed training, validation, and test accuracy [66]. In NASBench dataset, the neural network architectures have been exhaustively trained and evaluated on CIFAR-10 to create a queryable dataset. Each architecture training takes approximately 0.7 GPU hour.

NASBENCH201. NAS-Bench-201⁶ includes all possible architectures generated by 4 nodes and 5 associated operation options, which results in 15,625 neural cell candidates in total. The Nasbench201 dataset includes the tabular results for three subdatasets including CIFAR-10, CIFAR-100 and ImageNet-16-120. Each architecture training for Cifar10 takes approximately 0.7 GPU hours, Cifar100 takes 1.4 GPU hours and Imagenet takes 4 GPU hours.

⁵<https://github.com/google-research/nasbench>

⁶<https://github.com/D-X-Y/NAS-Bench-201>

D Proofs

D.1 Proof for Lemma 2.1

Proof. We consider $X \sim GP(m(), k())$. If k is not a p.s.d. kernel, then there is some set of n points $(t_i)_{i=1}^n$ and corresponding weights $\alpha_i \in \mathcal{R}$ such that

$$\sum_{i=1}^n \sum_{j=1}^n \alpha_i k(t_i, t_j) \alpha_j < 0. \quad (13)$$

By the GP assumption, $\text{Cov}(X(t_i), X(t_j)) = k(t_i, t_j)$, we show that the variance is now negative

$$\text{Var} \left(\sum_{i=1}^n \alpha_i X(t_i) \right) = \sum_{i=1}^n \sum_{j=1}^n \alpha_i \text{Cov}(X(t_i), X(t_j)) \alpha_j < 0. \quad (14)$$

The negative variance concludes our prove that the GP is no longer valid with non-p.s.d. kernel. ■

D.2 Proof for Proposition 1

Proof. We have that tree-Wasserstein (TW) is a metric and negative definite [30]. Therefore, $W_{d_{\mathcal{T}_o}}, W_{d_{\mathcal{T}_-}}, W_{d_{\mathcal{T}_+}}$ are also a metric and negative definite.

Moreover, the discrepancy d_{NN} is a convex combination with positive weights for $W_{d_{\mathcal{T}_o}}, W_{d_{\mathcal{T}_-}}, W_{d_{\mathcal{T}_+}}$. Therefore, it is easy to verify that for given neural networks $\mathbf{x}_1, \mathbf{x}_2, \mathbf{x}_3$, we have:

- $d_{\text{NN}}(\mathbf{x}_1, \mathbf{x}_1) = 0$.
- $d_{\text{NN}}(\mathbf{x}_1, \mathbf{x}_2) = d_{\text{NN}}(\mathbf{x}_2, \mathbf{x}_1)$.
- $d_{\text{NN}}(\mathbf{x}_1, \mathbf{x}_2) + d_{\text{NN}}(\mathbf{x}_1, \mathbf{x}_2) \geq d_{\text{NN}}(\mathbf{x}_2, \mathbf{x}_3)$.

Thus, d_{NN} is a pseudo-metric. Additionally, a convex combination with positive weights preserves the negative definiteness. Therefore, d_{NN} is negative definite. ■

D.3 Tree-Wasserstein kernel for neural networks

Proposition 3. *Given the scalar length-scale parameter σ_l^2 , the tree-Wasserstein kernel for neural networks $k(x, z) = \exp(-\frac{d_{\text{NN}}(x, z)}{\sigma_l^2})$ is infinitely divisible.*

Proof. Given two neural networks \mathbf{x} and \mathbf{z} , we introduce new kernels $k_\gamma(\mathbf{x}, \mathbf{z}) = \exp(-\frac{d_{\text{NN}}(\mathbf{x}, \mathbf{z})}{\gamma \sigma_l^2})$ for $\gamma \in \mathbb{N}^*$. Following [3] (Theorem 3.2.2, p.74), $k_\gamma(x, z)$ is also positive definite. Moreover, we also have $k(\mathbf{x}, \mathbf{z}) = (k_\gamma(\mathbf{x}, \mathbf{z}))^\gamma$. Then, following [3] (Definition 2.6, p.76), we complete the proof. ■

From Proposition 3, one does not need to recompute the Gram matrix of the TW kernel for each choice of σ_l^2 , since it suffices to compute it once.

E An example of TW computation for neural network architectures

In this section, we present an example of using TW for transporting two neural network architectures in Fig. 7. We consider a set \mathbb{S} of interest operations as follow $\mathbb{S} = \{\text{cv1, cv3, mp3}\}$.

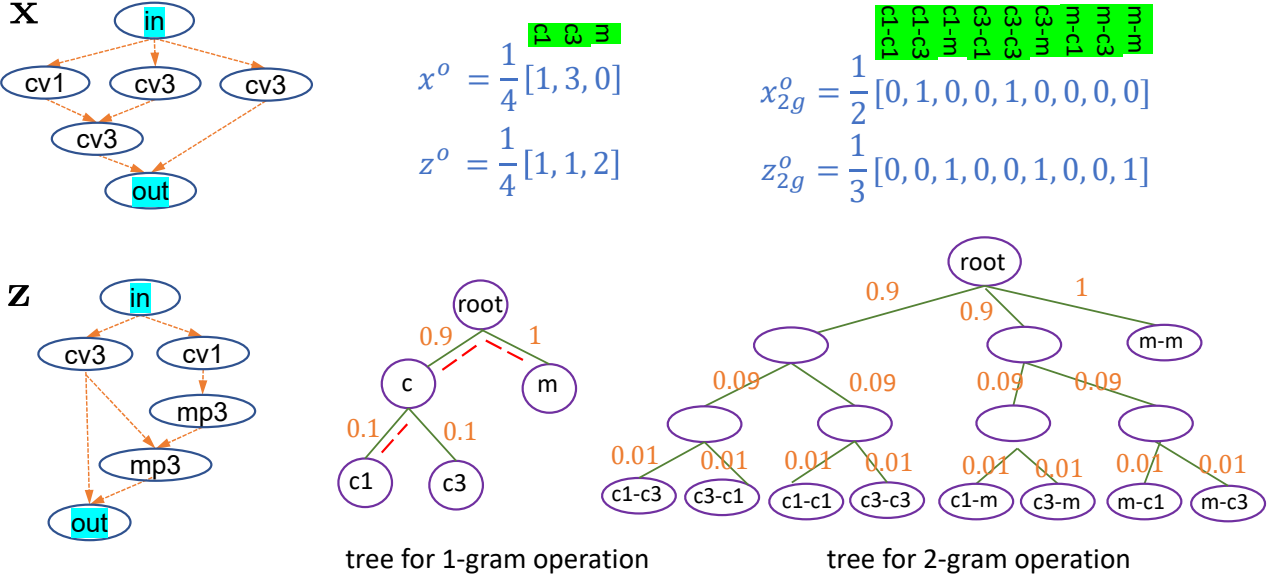


Figure 7: Example of TW used for calculating two architectures. The label of each histogram bin is highlighted in green. The distance between two nodes in a tree is sum of total cost if we travel between the two nodes, see Eq. (2). For example, the cost for moving `maxpool` (m) to `conv1` ($c1$) is $1 + 0.9 + 0.1 = 2$. We use similar analogy for computing in 2-gram (2g) representation.

Neural network information (\mathcal{S}^o, A). We use the order top-bottom and left-right for layers in \mathcal{S}^o .

- For neural network \mathbf{x} , we have $\mathcal{S}_{\mathbf{x}}^o = \{\text{in}, \text{cv1}, \text{cv3}, \text{cv3}, \text{out}\}$,

$$A_{\mathbf{x}} = \begin{pmatrix} 0 & 1 & 1 & 1 & 0 & 0 \\ 0 & 0 & 0 & 0 & 1 & 0 \\ 0 & 0 & 0 & 0 & 1 & 0 \\ 0 & 0 & 0 & 0 & 0 & 1 \\ 0 & 0 & 0 & 0 & 0 & 1 \\ 0 & 0 & 0 & 0 & 0 & 0 \end{pmatrix}$$

- For neural network \mathbf{z} , we have $\mathcal{S}_{\mathbf{z}}^o = \{\text{in}, \text{cv3}, \text{cv1}, \text{mp3}, \text{mp3}, \text{out}\}$,

$$A_{\mathbf{z}} = \begin{pmatrix} 0 & 1 & 1 & 0 & 0 & 0 \\ 0 & 0 & 0 & 0 & 1 & 1 \\ 0 & 0 & 0 & 1 & 0 & 0 \\ 0 & 0 & 0 & 0 & 1 & 0 \\ 0 & 0 & 0 & 0 & 0 & 1 \\ 0 & 0 & 0 & 0 & 0 & 0 \end{pmatrix}$$

We show how to calculate these three representations (layer operation, indegree and outdegree) using tree-Wasserstein.

E.1 n -gram representation for layer operations

- **1-gram representation.** The 1-gram representations \mathbf{x}_1^o and \mathbf{z}_1^o for neural network \mathbf{x} , and \mathbf{z} respectively are:

$$\mathbf{x}_1^o = \frac{1}{4}(1, 3, 0) \quad \mathbf{z}_1^o = \frac{1}{4}(1, 1, 2)$$

where we use the order (1:cv1, 2:cv3, 3:mp3) for the frequency of interest operations in the set \mathbb{S} for the 1-gram representation of neural network.

Table 1: The tree-metric for operations in $W_{d_{T_o}}$ from our predefined tree in Fig. 7 satisfying the following properties: (i) identical operation (cv1, cv1) has zero cost, (ii) similar operations (cv1, cv3) have small cost, and (iii) very different operations (cv1, mp3) have high cost. Then, the similarity score is normalized in Eq. (5) and Eq. (6) in which the weighting parameters α are learnt directly from the data. The utility score is further standardized $\mathcal{N}(0, 1)$ for robustness. Therefore, our model is robust to the choice of the predefined tree for the cost in this table. (Recall that the cost in the table is computed by tree metric (i.e., the length of the shortest path) between the pair-wise operations in the predefined tree in Fig. 7.)

	cv1	cv3	mp3
cv1	0	0.2	2
cv3	0.2	0	2
mp3	2	2	0

- **2-gram representation.** For the 2-gram representations \mathbf{x}_2^o and \mathbf{z}_2^o for neural networks \mathbf{x} and \mathbf{z} respectively, we use the following order for $\mathbb{S} \times \mathbb{S}$: (1:cv1-cv1, 2:cv1-cv3, 3:cv1-mp3, 4:cv3-cv1, 5:cv3-cv3, 6:cv3:mp3, 7:mp3-cv1, 8:mp3:cv3, 9:mp3-mp3). Thus, we have

$$\mathbf{x}_2^o = \frac{1}{2}(0, 1, 0, 0, 1, 0, 0, 0, 0), \quad \mathbf{z}_2^o = \frac{1}{3}(0, 0, 1, 0, 0, 1, 0, 0, 1).$$

Or, we can represent them as empirical measures

$$\omega_{\mathbf{x}_2^o} = \frac{1}{2}\delta_{\text{cv1-cv3}} + \frac{1}{2}\delta_{\text{cv3-cv3}}, \quad \omega_{\mathbf{z}_2^o} = \frac{1}{3}\delta_{\text{cv1-mp3}} + \frac{1}{3}\delta_{\text{cv3-mp3}} + \frac{1}{3}\delta_{\text{mp3-mp3}}.$$

- **Tree metrics for n -gram representations for layer operations.** We can use the tree metric in Fig. 7 for 1-gram and 2-gram representations. The tree metric for operations are summarized in Table 1.

Using the closed-form computation of tree-Wasserstein presented in Eq. (2) in the main text, we can compute $W_{d_{T_o}}(\mathbf{x}_1^o, \mathbf{z}_1^o)$ for 1-gram representation and $W_{d_{T_o}}(\mathbf{x}_2^o, \mathbf{z}_2^o)$ for 2-gram representation.

For 1-gram representation, we have

$$W_{d_{T_o}}(\mathbf{x}_1^o, \mathbf{z}_1^o) = 0.1 \left| \frac{1}{4} - \frac{1}{4} \right| + 0.1 \left| \frac{3}{4} - \frac{2}{4} \right| + 0.9 \left| 1 - \frac{3}{4} \right| + 1 \left| 0 - \frac{1}{4} \right| = 0.5. \quad (15)$$

For 2-gram representation, we have

$$\begin{aligned} W_{d_{T_o}}(\mathbf{x}_2^o, \mathbf{z}_2^o) = & 0.1 \left| \frac{1}{2} - 0 \right| + 0.1 \left| \frac{1}{2} - 0 \right| + 0.9 \left| 1 - 0 \right| \\ & + 0.01 \left| 0 - \frac{1}{3} \right| + 0.01 \left| 0 - \frac{1}{3} \right| + 0.99 \left| 0 - \frac{2}{3} \right| + 1 \left| 0 - \frac{1}{3} \right| = 2. \end{aligned} \quad (16)$$

E.2 Indegree and outdegree representations for network structure

The indegree and outdegree empirical measures $(\omega_{\mathbf{x}}^{d^-}, \omega_{\mathbf{x}}^{d^+})$ and $(\omega_{\mathbf{z}}^{d^-}, \omega_{\mathbf{z}}^{d^+})$ for neural networks \mathbf{x} and \mathbf{z} respectively are:

$$\omega_{\mathbf{x}}^{d^-} = \sum_{i=1}^6 \mathbf{x}_i^{d^-} \delta_{\frac{\eta_{\mathbf{x},i}+1}{M_{\mathbf{x}}+1}}, \quad \omega_{\mathbf{x}}^{d^+} = \sum_{i=1}^6 \mathbf{x}_i^{d^+} \delta_{\frac{\eta_{\mathbf{x},i}+1}{M_{\mathbf{x}}+1}} \quad (17)$$

$$\omega_{\mathbf{z}}^{d^-} = \sum_{i=1}^6 \mathbf{z}_i^{d^-} \delta_{\frac{\eta_{\mathbf{z},i}+1}{M_{\mathbf{z}}+1}}, \quad \omega_{\mathbf{z}}^{d^+} = \sum_{i=1}^6 \mathbf{z}_i^{d^+} \delta_{\frac{\eta_{\mathbf{z},i}+1}{M_{\mathbf{z}}+1}} \quad (18)$$

(η_l longest path length to root, d^- indegree, d^+ outdegree)

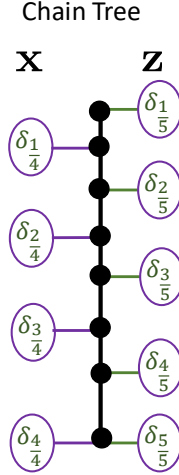
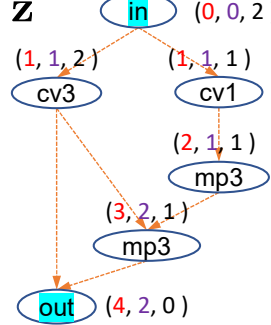
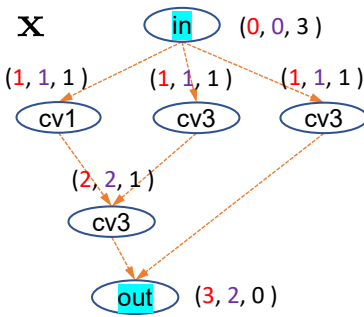


Figure 8: Illustration of indegree and outdegree used in TW. We can represent the empirical measure as $\omega_{\mathbf{x}}^{d^-} = \sum_{\ell \in L_{\mathbf{x}}} \mathbf{x}_{\ell}^{d^-} \delta_{\frac{\eta_{x_{\ell}, \ell}+1}{M_x+1}} = \frac{3}{7} \delta_{\frac{2}{4}} + \frac{2}{7} \delta_{\frac{3}{4}} + \frac{2}{7} \delta_{\frac{4}{4}}$ and $\omega_{\mathbf{x}}^{d^+} = \sum_{\ell \in L_{\mathbf{x}}} \mathbf{x}_{\ell}^{d^+} \delta_{\frac{\eta_{x_{\ell}, \ell}+1}{M_x+1}} = \frac{3}{7} \delta_{\frac{1}{4}} + \frac{3}{7} \delta_{\frac{2}{4}} + \frac{1}{7} \delta_{\frac{3}{4}}$ and for \mathbf{z} as $\omega_{\mathbf{z}}^{d^-} = \sum_{\ell \in L_{\mathbf{z}}} \mathbf{z}_{\ell}^{d^-} \delta_{\frac{\eta_{z_{\ell}, \ell}+1}{M_z+1}} = \frac{2}{7} \delta_{\frac{2}{5}} + \frac{1}{7} \delta_{\frac{3}{5}} + \frac{2}{7} \delta_{\frac{4}{5}} + \frac{2}{7} \delta_{\frac{5}{5}}$ and $\omega_{\mathbf{z}}^{d^+} = \sum_{\ell \in L_{\mathbf{z}}} \mathbf{z}_{\ell}^{d^+} \delta_{\frac{\eta_{z_{\ell}, \ell}+1}{M_z+1}} = \frac{2}{7} \delta_{\frac{1}{5}} + \frac{3}{7} \delta_{\frac{2}{5}} + \frac{1}{7} \delta_{\frac{3}{5}} + \frac{1}{7} \delta_{\frac{4}{5}}$. The tree, which is a chain $(1/5 \rightarrow 1/4 \rightarrow 2/5 \rightarrow 2/4 \rightarrow 3/5 \rightarrow 3/4 \rightarrow 4/5 \rightarrow 1)$, is used to compute the distance.

where

$$\mathbf{x}^{d^-} = \left(0, \frac{1}{7}, \frac{1}{7}, \frac{1}{7}, \frac{2}{7}, \frac{2}{7} \right), \quad \mathbf{x}^{d^+} = \left(\frac{3}{7}, \frac{1}{7}, \frac{1}{7}, \frac{1}{7}, \frac{1}{7}, 0 \right), \quad (19)$$

$$\mathbf{z}^{d^-} = \left(0, \frac{1}{7}, \frac{1}{7}, \frac{1}{7}, \frac{2}{7}, \frac{2}{7} \right), \quad \mathbf{z}^{d^+} = \left(\frac{2}{7}, \frac{2}{7}, \frac{1}{7}, \frac{1}{7}, \frac{1}{7}, 0 \right), \quad (20)$$

$$\eta_{\mathbf{x}} = (0, 1, 1, 1, 2, 3), \quad \eta_{\mathbf{z}} = (0, 1, 1, 2, 3, 4), \quad (21)$$

$M_{\mathbf{x}} = 3$, $M_{\mathbf{z}} = 4$, and $\mathbf{x}_i^{d^-}, \mathbf{x}_i^{d^+}, \eta_{\mathbf{x}, i}$ are the i^{th} elements of $\mathbf{x}^{d^-}, \mathbf{x}^{d^+}, \eta_{\mathbf{x}}$ respectively. Consequently, one can leverage the indegree and outdegree for network structures to distinguish between \mathbf{x} and \mathbf{z} .

We demonstrate in Fig. 8 how to calculate the tree-Wasserstein for indegree and outdegree. The supports of empirical measures $\omega_{\mathbf{x}}^{d^-}$ and $\omega_{\mathbf{z}}^{d^-}$ are in a line. So, we simply choose a tree as a chain of real values for the tree-Wasserstein distance⁷. Particularly, the tree-Wasserstein is equivalent to the univariate optimal transport. It is similar for empirical measures $\omega_{\mathbf{x}}^{d^+}$ and $\omega_{\mathbf{z}}^{d^+}$.

- $W_{d_{\mathcal{T}}^-}(\omega_{\mathbf{x}}^{d^-}, \omega_{\mathbf{z}}^{d^-})$ for indegree representation. Using Eq. (2) we have

$$\begin{aligned} W_{d_{\mathcal{T}}^-}(\omega_{\mathbf{x}}^{d^-}, \omega_{\mathbf{z}}^{d^-}) &= \left(\frac{1}{4} - \frac{1}{5} \right) \underbrace{\left| \frac{7}{7} - \frac{7}{7} \right|}_{\Gamma\left(\delta_{\frac{1}{4}}\right)} + \left(\frac{2}{5} - \frac{1}{4} \right) \underbrace{\left| \frac{7}{7} - \frac{7}{7} \right|}_{\Gamma\left(\delta_{\frac{2}{5}}\right)} + \left(\frac{2}{4} - \frac{2}{5} \right) \underbrace{\left| \frac{7}{7} - \frac{5}{7} \right|}_{\Gamma\left(\delta_{\frac{2}{4}}\right)} + \left(\frac{3}{5} - \frac{2}{4} \right) \underbrace{\left| \frac{4}{7} - \frac{5}{7} \right|}_{\Gamma\left(\delta_{\frac{3}{5}}\right)} \\ &+ \left(\frac{3}{5} - \frac{2}{4} \right) \underbrace{\left| \frac{4}{7} - \frac{4}{7} \right|}_{\Gamma\left(\delta_{\frac{3}{4}}\right)} + \left(\frac{3}{5} - \frac{2}{4} \right) \underbrace{\left| \frac{2}{7} - \frac{4}{7} \right|}_{\Gamma\left(\delta_{\frac{4}{5}}\right)} + \left(\frac{3}{5} - \frac{2}{4} \right) \underbrace{\left| \frac{2}{7} - \frac{2}{7} \right|}_{\Gamma\left(\delta_{\frac{1}{1}}\right)} = \frac{4}{70} = 0.0571 \end{aligned} \quad (22)$$

where for each value $(t_1 - t_2) |a_1 - a_2|$, the value in the parenthesis, e.g., $(t_1 - t_2)$, is defined as the edge weights from δ_{t_1} to δ_{t_2} in Fig. 8 and the values in the absolute difference, e.g., $|a_1 - a_2|$ is the total mass of empirical measures in the subtrees rooted as the deeper node (i.e., δ_{t_2}) of corresponding edge (from δ_{t_1} to δ_{t_2}) as defined in Eq. (2).

⁷The tree is simply a chain of increasing real values, i.e., a chain $\frac{1}{3} \rightarrow \frac{2}{3} \rightarrow 1$, the weight in each edge is simply the ℓ_1 distance between two nodes of that edge.

- $W_{d_{\mathcal{T}_+}}(\omega_{\mathbf{x}}^{d^+}, \omega_{\mathbf{z}}^{d^+})$ for outdegree representation. Similarly, for outdegree representation, we have

$$\begin{aligned}
 W_{d_{\mathcal{T}_+}}(\omega_{\mathbf{x}}^{d^+}, \omega_{\mathbf{z}}^{d^+}) &= \left(\frac{1}{4} - \frac{1}{5}\right) \underbrace{\left|\frac{7}{7} - \frac{5}{7}\right|}_{\Gamma\left(\delta_{\frac{1}{4}}\right)} + \left(\frac{2}{5} - \frac{1}{4}\right) \underbrace{\left|\frac{4}{7} - \frac{5}{7}\right|}_{\Gamma\left(\delta_{\frac{2}{5}}\right)} + \left(\frac{2}{4} - \frac{2}{5}\right) \underbrace{\left|\frac{4}{7} - \frac{2}{7}\right|}_{\Gamma\left(\delta_{\frac{2}{4}}\right)} + \left(\frac{3}{5} - \frac{2}{4}\right) \underbrace{\left|\frac{1}{7} - \frac{2}{7}\right|}_{\Gamma\left(\delta_{\frac{3}{5}}\right)} \\
 &+ \left(\frac{3}{5} - \frac{2}{4}\right) \underbrace{\left|\frac{1}{7} - \frac{1}{7}\right|}_{\Gamma\left(\delta_{\frac{3}{4}}\right)} + \left(\frac{3}{5} - \frac{2}{4}\right) \underbrace{\left|\frac{0}{7} - \frac{1}{7}\right|}_{\Gamma\left(\delta_{\frac{4}{5}}\right)} + \left(\frac{3}{5} - \frac{2}{4}\right) \underbrace{\left|\frac{0}{7} - \frac{0}{7}\right|}_{\Gamma\left(\delta_1\right)} = \frac{6}{70} = 0.0857. \tag{23}
 \end{aligned}$$

From $W_{d_{\mathcal{T}_o}}$, $W_{d_{\mathcal{T}_-}}$ and $W_{d_{\mathcal{T}_+}}$, we can obtain the discrepancy d_{NN} between neural networks \mathbf{x} and \mathbf{z} as in Eq. (5) with predefined values $\alpha_1, \alpha_2, \alpha_3$.

F Optimizing hyperparameters in TW and GP

As equivalence, we consider $\lambda_1 = \frac{\alpha_1}{\sigma_t^2}$, $\lambda_2 = \frac{\alpha_2}{\sigma_t^2}$ and $\lambda_3 = \frac{1-\alpha_1-\alpha_2}{\sigma_t^2}$ in Eq. (6) and present the derivative for estimating the variable λ in our kernel.

$$k(\mathbf{u}, \mathbf{v}) = \exp\left(-\lambda_1 W_{d_{\mathcal{T}_o}}(\mathbf{u}, \mathbf{v}) - \lambda_2 W_{d_{\mathcal{T}_-}}(\mathbf{u}, \mathbf{v}) - \lambda_3 W_{d_{\mathcal{T}_+}}(\mathbf{u}, \mathbf{v})\right). \tag{24}$$

The hyperparameters of the kernel are optimised by maximising the log marginal likelihood (LML) of the GP surrogate

$$\theta^* = \arg \max_{\theta} \mathcal{L}(\theta, \mathcal{D}), \tag{25}$$

where we collected the hyperparameters into $\theta = \{\lambda_1, \lambda_2, \lambda_3, \sigma_n^2\}$. The LML and its derivative are defined as [43]

$$\mathcal{L}(\theta) = -\frac{1}{2} \mathbf{y}^\top \mathbf{K}^{-1} \mathbf{y} - \frac{1}{2} \log |\mathbf{K}| + \text{constant} \tag{26}$$

$$\frac{\partial \mathcal{L}}{\partial \theta} = \frac{1}{2} \left(\mathbf{y}^\top \mathbf{K}^{-1} \frac{\partial \mathbf{K}}{\partial \theta} \mathbf{K}^{-1} \mathbf{y} - \text{tr} \left(\mathbf{K}^{-1} \frac{\partial \mathbf{K}}{\partial \theta} \right) \right), \tag{27}$$

where \mathbf{y} are the function values at sample locations and \mathbf{K} is the covariance matrix of $k(\mathbf{x}, \mathbf{x}')$ evaluated on the training data.

optimization of the LML was performed via multi-started gradient descent. The gradient in Eq. (27) relies on the gradient of the kernel k w.r.t. each of its parameters:

$$\frac{\partial k(\mathbf{u}, \mathbf{v})}{\partial \lambda_1} = -W_{d_{\mathcal{T}_o}}(\mathbf{u}, \mathbf{v}) \times k(\mathbf{u}, \mathbf{v}) \tag{28}$$

$$\frac{\partial k(\mathbf{u}, \mathbf{v})}{\partial \lambda_2} = -W_{d_{\mathcal{T}_-}}(\mathbf{u}, \mathbf{v}) \times k(\mathbf{u}, \mathbf{v}) \tag{29}$$

$$\frac{\partial k(\mathbf{u}, \mathbf{v})}{\partial \lambda_3} = -W_{d_{\mathcal{T}_+}}(\mathbf{u}, \mathbf{v}) \times k(\mathbf{u}, \mathbf{v}). \tag{30}$$

F.1 Proof for Proposition 2

Proof. Let A and B be the training and test set respectively, we utilize the Schur complement to have $K_{A \cup B} = K_A \times [K_B - K_{BA}K_A^{-1}K_{AB}]$ and the probability of selecting B is

$$P(B \subset \mathcal{P} | A) = \frac{\det(K_{A \cup B})}{\det(K_A)} = \det(K_B - K_{BA}K_A^{-1}K_{AB}) = \det(\sigma(B | A)). \tag{31}$$

This shows that the conditioning of k-DPP is equivalent to the GP predictive variance $\sigma(B | A)$ in Eq. (9). ■

Table 2: Properties comparison across different distances for using with GP-BO and k-DPP. GW is Gromov-Wasserstein. TW is tree-Wasserstein. OT is optimal transport.

Representation	Matrix/Graph	Path-Encode	OT (or W)	GW	TW
Closed-form estimation	✓	✓	✗	✗	✓
Positive semi definite	✓	✓	✗	✗	✓
Different architecture sizes	✓, ✗	✗	✓	✓	✓
Scaling with architecture size	✓	✗	✓	✓	✓

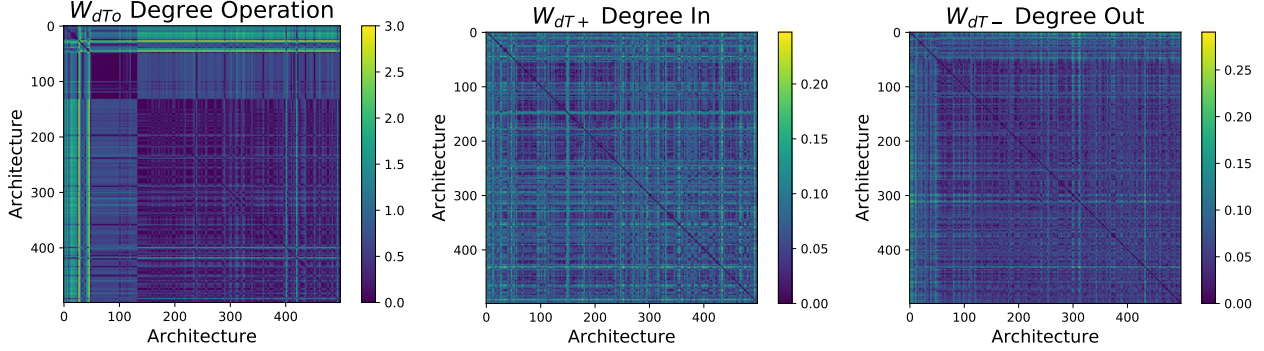


Figure 9: Tree-Wasserstein distances over 500 architectures on NASBENCH101.

G Distance Properties Comparison

We summarize the key benefits of using tree-Wasserstein (n-gram) as the main distance with GP for sequential NAS and k-DPP for batch NAS in Table 2. Tree-Wasserstein offers close-form computation and positive semi-definite covariance matrix which is critical for GP and k-DPP modeling.

Comparison with graph kernel. Besides the adjacency matrix representation, each architecture include layer masses and operation type. We note that two different architectures may share the same adjacency matrix while they are different in operation type and layer mass.

Comparison with path-based encoding. TW can scale well to more number of nodes, layers while the path-based encoding is limited to.

Comparison with OT approaches in computational complexity. In general, OT is formulated as a linear programming problem and its computational complexity is super cubic in the size of probability measures [6] (e.g., using network simplex). On the other hand, TW has a closed-form computation in Eq. (2), and its computational complexity is linear to the number of edges in the tree. Therefore, TW is much faster than OT in applications [30], and especially useful for large-scale settings where the computation of OT becomes prohibited.

H Additional Experiments and Illustrations

H.1 Model Analysis

We illustrate three internal distances of our tree-Wasserstein including $W_{d_{T_o}}$, $W_{d_{T_+}}$, $W_{d_{T_-}}$ in Fig. 9. Each internal distance captures different aspects of the networks. The zero diagonal matrix indicates the correct estimation of the same neural architectures.

H.2 Further sequential and batch NAS experiments

To complement the results presented in the main paper, we present additional experiments on both sequential and batch NAS setting using NB101 and NB201 dataset. in Fig. 10 We present additional experiments on batch

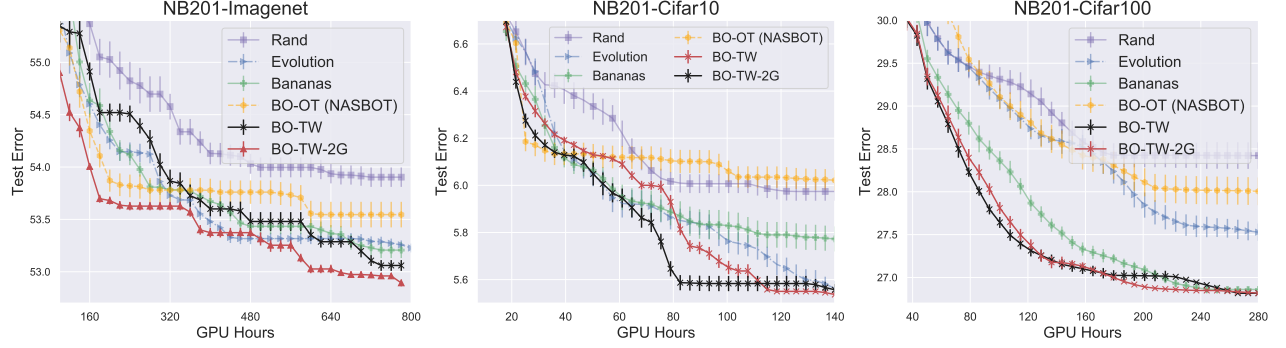


Figure 10: Additional sequential NAS comparison on NASBENCH201.

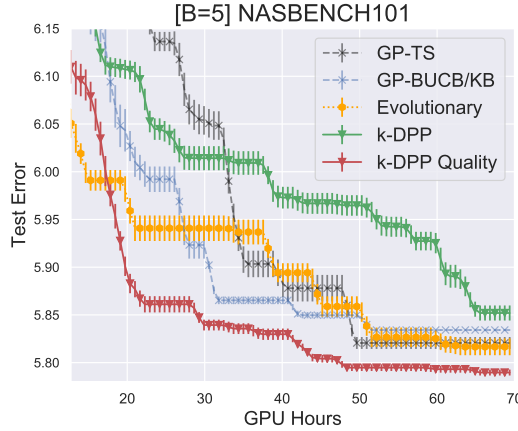


Figure 11: Additional result of batch NAS on NB101. We use TW-2G and a batch size $B = 5$

NAS settings in Fig. 11 that the proposed k-DPP quality achieves consistently the best performance.

H.3 Ablation study using different acquisition functions

We evaluate our proposed model using two common acquisition functions including UCB and EI. The result suggests that UCB tends to perform much better than EI for our NAS setting. This result is consistent with the comparison presented in Bananas [62].

H.4 Ablation study with different batch size B

Finally, we study the performance with different choices of batch size B in Fig. 13 which naturally confirms that the performance increases with larger batch size B .

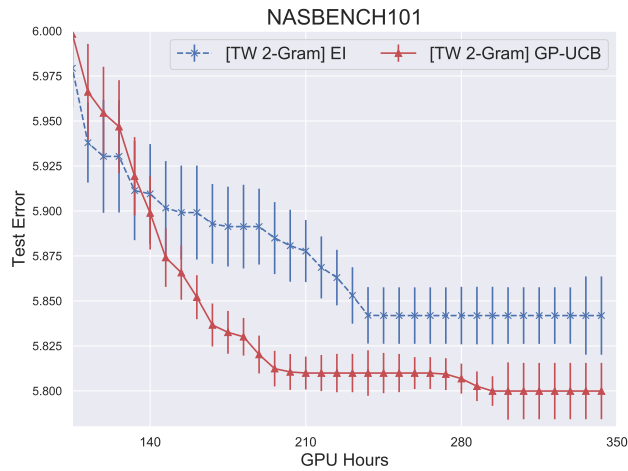


Figure 12: Optimizing the acquisition function using GP-UCB and EI on NB101. The results suggest that using GP-UCB will lead to better performance than EI.

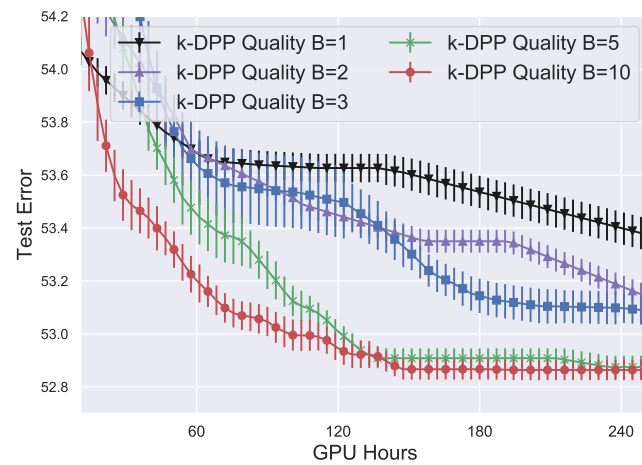


Figure 13: Performance with different batch sizes B on Imagenet. The result shows that the performance increases with larger batch size B , given the same wall-clock time budget (or batch iteration).